LIFETIME MEASUREMENT OF $\pi^+\pi^-$ AND $\pi^\pm K^\mp$ ATOMS TO TEST LOW ENERGY QCD

Letter of Intent of the experiment at Japan Proton Accelerator Research Complex

B. Adeva[l], L. Afanasyev[i], Z. Berka[b], V. Brekhovskikh[k], G. Caragheorgheopol[j], T. Cechak[b], M. Chiba[h], S. Constantinescu[j], A. Doudarev[i], D. Drijard[a], A. Gorin[k], O. Gortchakov[i], C. Guaraldo[d], M. Jabitski[i], V. Karpukhin[i], J. Kluson[b], M. Kobayashi[f], B. Kopeliovich[i], A. Koulikov[i], A. Kouptsov[i], V. Krouglov[i], L. Krouglova[i], K.-I. Kuroda[i], A. Lanaro[d], R. Lednicky[c], I. Manuilov[k], L. Nemenov[i], M. Nikitin[i], K. Okada[g], V. Olchevskii[i], M. Pentia[j], A. Penzo[e], A. Riazantsev[k], V. Rykalin[k], J. Schacher[n], J. Smolik[c], F. Takeutchi[g], A. Tarasov[i], L. Tauscher[m], T. Trojek[b], S. Trousov[o], V. Yazkov[o], P. Zrelov[i]

[a] CERN, Geneva, Switzerland
[b] Czech Technical University, Prague, Czech Republic
[c] Institute of Physics ASCR, Prague, Czech Republic
[d] INFN - Laboratori Nazionali di Frascati, Frascati, Italy
[e] Trieste University and INFN-Trieste, Italy
[f] KEK, Tsukuba, Japan
[g] Kyoto Sangyou University, Japan
[h] Tokyo Metropolitan University, Japan
[i] JINR Dubna, Russia
[j] National Institute for Physics and Nuclear Engineering IFIN-HH, Bucharest, Romania
[k] IHEP Protvino, Russia
[l] Santiago de Compostela University, Spain
[m] Basel University, Switzerland
[n] Bern University, Switzerland
[o] Skobeltsyn Institute for Nuclear Physics of Moscow State Univeristy

Contact person: L.Nemenov,
e-mail: Leonid.Nemenov@cern.ch, tel.:+41-22-7673044, fax: +41-22-7679475

Abstract

The proposed experiment aims to measure simultaneously the lifetime of $\pi^+\pi^-$ atoms ($A_{2\pi}$) and πK atoms ($A_{\pi K}$) in the ground state using 30 (50) GeV proton beam of Japan Proton Accelerator Research Complex (J-PARC).

The precise measurement of this quantities enables to determine in a model-independent way the combination of s-wave pion-pion $|a_0 - a_2|$ and pion-kaon $|a_{1/2} - a_{3/2}|$ scattering lengths (with isospin 0, 2 and 1/2, 3/2, respectively). The precision of $A_{2\pi}$ lifetime measurement will be on the level of 6% and the difference $|a_0 - a_2|$ will be determined on the level of 3%. The accuracy of $A_{\pi K}$ lifetime measurement will be on the level of 24% and the difference $|a_{1/2} - a_{3/2}|$ will be determined on the level of 12%.

Low energy QCD provides for these values an accuracy about 2% for the pion-pion scattering lengths and about 10% of the πK-scattering lengths. These results have been obtained assuming a strong condensation of quark-antiquark pairs in vacuum.

The pion-pion and pion-kaon scattering lengths have never been confronted with experimental data on the level of theoretical precision. On this reason the proposed measurements will be a crucial check of the low energy QCD predictions and our understanding of the nature of QCD vacuum.

In the proposed experiment the very thin targets will be used and a required luminosity can be obtained at interaction with the proton beam halo only. Thus, the setup can be installed upsteam of all other targets in the K-hall and can work all time without disturbing other experiments.

Contents

1 Physical motivation

1.1 Decay of $\pi^+\pi^-$ atom as a source of information on the pion scattering lengths

In the case of hadronic atoms a measurement of the lifetime τ (decay rate) allows to determine a combination of S-wave scattering lengths for the particles, which constitute the atom [1].

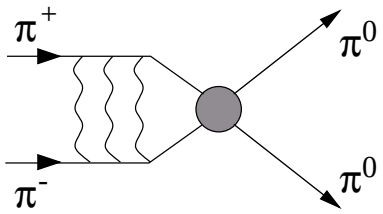

Figure 1: The dominant decay channel of *pionium*.

Using the framework of low energy QCD the decay of $A_{2\pi}$ atom $A_{2\pi}(ground\ state) \to \pi^0\pi^0$ (Fig.1) is characterised by the decay rate or inverse lifetime [2, 3, 4, 5, 6, 7]

$$\Gamma_{2\pi^0} = \frac{1}{\tau} = \frac{2}{9}\,\alpha^3\,p\,|a_0 - a_2|^2\ (1+\delta). \tag{1}$$

Here, α is the fine structure constant, $p = \left(M_{\pi^+}^2 - M_{\pi^0}^2 - \frac{1}{4}M_{\pi^+}^2\alpha^2\right)^{1/2}$ is the π^0 momentum in the pionium system, M_{π^+} and M_{π^0} are the masses of π^+ and π^0, respectively, and a_0 and a_2 are the S-wave $\pi\pi$ scattering lengths for isopin $I = 0$ and 2, respectively. The term δ, which accounts for corrections of order α as well as for those due to $m_u \neq m_d$, is a known quantity ensuring a 1% accuracy for equation (1) [6]. As seen in (1) a measurement of the lifetime τ allows to obtain in a model-independent way a value of $|a_0 - a_2|$.

1.2 Theoretical status

The $\pi\pi$ scattering lengths a_0, a_2 have been calculated by means of an effective Lagrangian and Chiral Perturbation Theory [8] with a precision better than 2.5% [9, 10]:

$$a_0 = 0.220 \pm 0.005\,, \quad a_2 = 0.0444 \pm 0.0010\,, \quad a_0 - a_2 = 0.265 \pm 0.004\,. \tag{2}$$

Here the scattering lengths are given in units of $M_{\pi^+}^{-1}$. Hence the lifetime of $A_{2\pi}$ in the ground state is predicted to be

$$\tau = (2.9 \pm 0.1) \cdot 10^{-15}\,\mathrm{s}\,. \tag{3}$$

These results are based on the assumption that the spontaneous chiral symmetry breaking is due to a strong quark condensate [11]. An alternative scenario with an arbitrary value of the quark condensate [12] admits larger a_0, a_2 compared to those of the standard scheme [10]. This is the reason why a measurement of scattering lengths provides an opportunity to verify the current understanding of chiral symmetry breaking in QCD and to check the magnitude of the quark condensate.

1.3 Experimental status of pion scattering lengths

The value of a_0 was obtained from detailed investigation of the decay $K \to \pi^+\pi^- e^+\nu_e$ with precision of 18%: $a_0 = 0.28 \pm 0.05$ [13]. The analysis of that data combined with the Roy equation and the inclusion of peripheral $\pi N \to \pi\pi N$ data led to the presently accepted value of $a_0 = 0.26 \pm 0.05$ [14]. The most recent result of the experiment E865 from the K_{e4} decay [15] — $a_0 = 0.216 \pm 0.013(\mathrm{stat}) \pm 0.004(\mathrm{syst}) \pm 0.005(\mathrm{theor})$ — was obtained essentially exploiting results of the Chiral Perturbation Theory. This results still do not reach the accuracy of the theoretical prediction and in other planned experiments on the K_{e4} decay the expected accuracy will be on the same level.

In the DIRAC experiment [16] the expected statistical accuracy of $|a_0 - a_2|$ will be about 6%. This value is 4 time larger than the correspondent theoretical accuracy (2).

1.4 Decay of πK atom and πK scattering lengths

The dominant decay process for $A_{\pi K}$ atoms is:

$$A_{\pi K} \to \pi^0 + \overline{K^0}. \tag{4}$$

For $A_{\pi K}$ with principal quantum number *n* and orbital angular momentum *l*=0, the probability for this transition at leading order of isospin breaking is given by the following expression [17]:

$$\Gamma_{n,0}(\pi^0\overline{K^0}) = \frac{1}{\tau_{n,0}} \approx \frac{8\pi}{9}\left(\frac{2\Delta m}{\mu}\right)^{1/2}(a_{1/2} - a_{3/2})^2|\Psi_{n,0}(0)|^2 + \cdots \tag{5}$$

where $\Delta m = (M_{K^-} + M_{\pi^+}) - (M_{\pi^0} + M_{\overline{K^0}})$, $\mu = \dfrac{M_{K^-}\, M_{\pi^+}}{M_{K^-} + M_{\pi^+}}$ is the reduced atomic mass and $\Psi_{n,0}$ is the Coulomb wave function of $A_{\pi K}$ at zero distance. The ellipsis denote isospin breaking corrections, which could be evaluated in the same way as done for the $A_{2\pi}$ decay probability [18, 19, 20, 21, 22]. These corrections for $A_{\pi K}$ have not yet been worked out. Nevertheless, it is expected that they can be determined rather precisely improving the accuracy of Eq. (5) to few percent [23]. Corrections to the $A_{2\pi}$ lifetime have been studied also in a potential approach [24, 25], and the same procedure is applicable to $A_{\pi K}$.

Substituting the πK scattering length values from (7) into Eq. (5), one obtains, at leading order in isospin breaking, the $A_{\pi K}$ lifetime in the ground state

$$\tau_{1,0} \equiv \tau = 4.7 \cdot 10^{-15}\ \mathrm{s}. \tag{6}$$

Therefore if one measures τ with precision of 24% the difference $|a_{1/2} - a_{3/2}|$ will be known up to 12%.

For the S-wave πK scattering lengths with isospin 1/2 and 3/2 the following values in units of $M_{\pi^+}^{-1}$ have been predicted [26]:

$$a_{1/2} = 0.19 \pm 0.02; \qquad a_{3/2} = -0.05 \pm 0.02. \tag{7}$$

The errors in (7) are due to the uncertainties of the low energy constants and to higher order corrections ($\mathcal{L}_{(6)}$ and two-loops). A recent calculation [27] lead to a more precise value of

$$a_{1/2} - a_{3/2} = 0.23 \pm 0.01, \tag{8}$$

Table 1: *πK scattering lengths determined by using dispersion relations.*

Reference	[28]	[29]	[30]
$a_{1/2}$	0.237	0.240 ± 0.002	0.13 ± 0.09
$a_{3/2}$	-0.074	-0.05 ± 0.06	-0.13 ± 0.03

in good agreement with the previous ones.

Later experiments (see Table 1) have determined the behaviour of πK scattering near threshold using advanced methods based on dispersion relations. Unfortunately, the results are still not free from inconsistencies.

As can be seen from the results above, threshold parameters of πK scattering are known with a low accuracy. According to table 1 containing data, evaluated by using dispersion relation techniques, the experimental values for $a_{1/2}$ lie in the range 0.13 to 0.24 and for $a_{3/2}$ in -0.13 to -0.05. This means, that these values are only known within a factor 2. New precise measurements of πK threshold parameters are strongly needed in order to improve the understanding of πK processes. One possibility would be to measure the πK-atom lifetime and then to extract the difference $|a_{1/2} - a_{3/2}|$. In ref. [30], exactly this scattering length combination was determined taking advantage of the forward sum rule and exploiting measured phase shifts. The allowed range of values was found to be $0.21 \leq a_{1/2} - a_{3/2} \leq 0.32 \ \left(M_{\pi^+}^{-1}\right)$. After 30 years of experimental study and after tremendous progress in theory (ChPT), a direct as well as more precise measurement of this quantity is quite required. As pointed out in ref. [26], more precise empirical information on the threshold parameters of πK scattering would give us a chance to test crucially the low-energy structure of QCD.

2 Detection of relativistic $A_{2\pi}$ and lifetime measurement

2.1 Measurement with single target

The method for detecting $A_{2\pi}$ is based on the observation of $\pi\pi$ pairs from the atom breakup (ionisation) which occurs in the production target. The breakup probability is the ratio between the number of ionised (n_A) and the number of produced (N_A) $A_{2\pi}$:

$$P_{\rm br} = n_A / N_A \,. \tag{9}$$

The main feature of these "atomic" pairs is their low relative momentum Q in the centre of mass system ($Q < 4$ MeV/c). For a given target thickness and $A_{2\pi}$ momentum, the breakup probability of the $\pi^+\pi^-$ atom is a unique function of τ, the lifetime in the ground state [37]. Therefore, the measurement of the breakup probability allows to investigate the atom lifetime [31].

All detected $\pi^+\pi^-$ pairs produced in the target includes pairs of real and accidental coincidences:

$$N = N_{\rm real} + N_{\rm acc} \,. \tag{10}$$

Next, the "real" pairs consist of pairs produced in the free states and "atomic" pairs:

$$N_{\rm real} = N_{\rm free} + n_A \,. \tag{11}$$

The "free" pairs can be separated in respect to a size of their production region:

$$N_{\rm free} = N_{\rm C} + N_{\rm nC}\,. \tag{12}$$

Here $N_{\rm C}$ is the number of so called "Coulomb" pairs originating from short-lived sources (ρ, K^*, ϕ, fragmentation, ...: fig. 2c) and affected by the strong and more significantly the Coulomb interaction in the final state. $N_{\rm nC}$ is the number of $\pi^+\pi^-$ pairs with at least one particle originating from long-lived sources (η, η',...: fig. 2b) and so they are called as "non-Coulomb" pairs.

Accidental $\pi^+\pi^-$ pairs are uncorrelated in time (fig. 2a), i.e. they are neither affected by Coulomb nor strong interaction in the final state. We use them to describe the distribution of free $\pi^+\pi^-$ pairs. If we denote the Q distribution of accidental pairs as $dN_{\rm acc}/dQ \equiv \Phi(Q)$, then the distribution of real $\pi^+\pi^-$ pairs $dN_{\rm free}/dQ$ can be approximated as follows:

$$\begin{aligned} dN_{\rm free}/dQ &= \underbrace{A\Phi(Q)}_{\rm long} + \underbrace{B\Phi(Q)(1+aQ)A_C(Q)}_{\rm short} = \\ &= B\Phi(Q)\left[(1+aQ)A_C(Q) + f\right], \qquad f = A/B \end{aligned} \tag{13}$$

where the terms $(1+aQ)$ and $A_C(Q)$ take into account strong and Coulomb final-state interactions, respectively [32]. The Coulomb correlation function, $A_C(Q)$, is known from theory with a precision of $\sim 0.5\%$ [33], whereas B, a, f are free parameters, and $\Phi(Q)$ is the measured spectrum of accidentals.

The experimental distribution $dN_{\rm real}/dQ$ of real $\pi^+\pi^-$ pairs is fitted by the function (13) for values $Q > 4\,$MeV/c, where no "atomic" pairs are expected. The values of the fit parameters B, a and f are then used to determine the total number of free pairs in the region $Q \leq 3\,$MeV/c. Finally, the number of "atomic" pairs n_A in the interval $Q \leq 3\,$MeV/c is obtained by subtracting $N_{\rm free}$ from the total number of $\pi^+\pi^-$ pairs collected in this interval.

From the best values of the fit parameters B a and f, we can also determine the total number of "Coulomb" pairs ($N_{\rm C}$) in the region $Q \leq 3\,$MeV/c. The strong part in the production of the "Coulomb" pairs with $Q \leq 3\,$MeV/c as well as in the production of $A_{2\pi}$ is the same (fig. 3) and so cancels out in the ratio $N_A/N_{\rm C}$. Therefore, the number of produced $A_{2\pi}$, N_A, can be

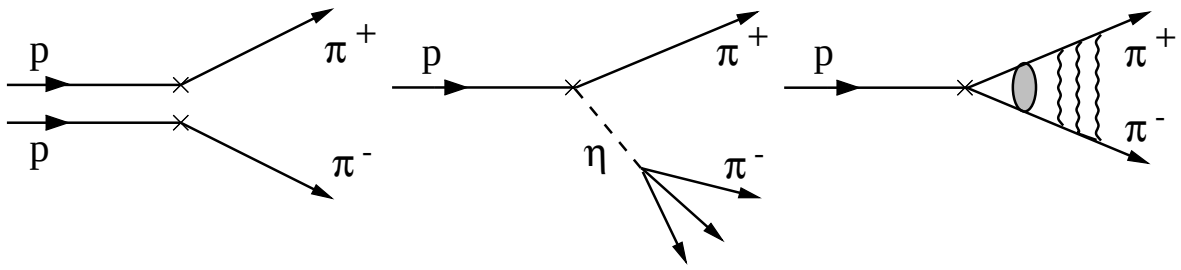

$\frac{dN_{\rm acc}}{dQ} \sim \Phi(Q)$ (a) $\quad \frac{dN_{\rm nC}}{dQ} \sim \Phi(Q)$ (b) $\quad \frac{dN_{\rm C}}{dQ} \sim \Phi(Q)(1+kQ)A_C(Q)$ (c)

Figure 2: *Production diagrams: (a) accidental pairs, (b) pairs from long-lived sources, (c) pairs from short-lived sources. Accidental pairs and pairs originating from long-lived sources have the same Q distribution in the region of low Q, at least for $Q \leq 30\,$MeV/c.*

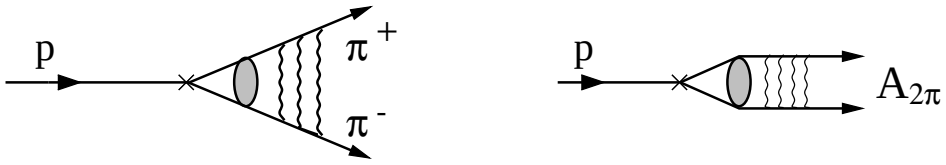

(a) (b)

Figure 3: *Diagrams of "Coulomb" pairs (a) and $A_{2\pi}$ (b) production. Both have the same strong production contribution for $Q \leq 3$ MeV/c*

determined in the model-independent way [34, 35], *i.e.* via the relation:

$$N_A = kN_{\rm C} = 0.615N_{\rm C}(Q \leq 2\,{\rm MeV}/c) \tag{14}$$

This procedure was used in our previous experiment, where first experimental evidence for $A_{2\pi}$ was found and a lifetime estimation was made [36] and later in DIRAC [16].

The lifetime dependence of the $A_{2\pi}$ breakup probability $P_{\rm br}^{\rm th}(\tau)$ can be calculated with a precision $\sim 1\%$ for any target [38, 39, 40, 41, 42, 43]. The $A_{2\pi}$ lifetime, τ, can be determined by comparing the measured value, $P_{\rm br}^{\rm exp} = n_A/N_A$, with the theoretical curve $P_{\rm br}^{\rm th}(\tau)$ (see Fig. 4 for $L = 1$).

2.2 The two target method for the lifetime measurement

The method is based on measurements with two different target types: 1) single-layer target and 2) multi-layer target of the same total thickness, but consisting of a few layers with 1 mm gaps in between. The main idea is to provide a "pure" experimental observation of $\pi^+\pi^-$ pairs from $A_{2\pi}$ breakup in the target and an alternative method of the lifetime measurements.

Production of all $\pi^+\pi^-$ pairs in these two targets will be the same excluding "atomic" pairs. The probability of $A_{2\pi}$ breakup in the multi-layer targets is lower and its dependence on the lifetime is much weaker than for the single-layer target (see Fig. 4). Thus, the difference between the observed distributions obtained with these two targets should only contain "atomic" pairs and their number depends on the atom lifetime τ.

Let us consider the following combination of the numbers of "real" events (see Eq.11) in the range of small relative momentum for these two targets, assuming the same number of the proton interactions in both targets:

$$V(\tau) = \frac{N_{\rm real}^s - N_{\rm real}^m}{N_{\rm C}} = \frac{n_A^s - n_A^m}{N_A/k} = \frac{kN_A(P_{\rm br}^s - P_{\rm br}^m)}{N_A} = k(P_{\rm br}^s(\tau) - P_{\rm br}^m(\tau))\ . \tag{15}$$

Here indices s and m denote values related to the single- and multi-layer targets; $N_{\rm C}$ is number of "Coulomb" pairs extracted from the fit procedure described above in Sect. 2.1 and k comes from the relation $N_A = kN_C$ (see Eq.14). The dependences of the function $V(\tau)$ on the lifetime τ are shown in Fig. 5.

To compare two methods of the lifetime measurements the theoretical values of $P_{\rm br}(\tau)$ and the data collected in 2001 with the Nickel target have been used: $N_{\rm real} = 17696 \pm 135$, $N_{\rm C} = 13763 \pm 250$ and $n_A = 3265 \pm 259$. To simulate n_A for multi-layer target the measured value have been corrected according to $P_{\rm br}$ values. Summarized values are given in the Table 2. The first column contains information for the single-target method, all others for the two-target

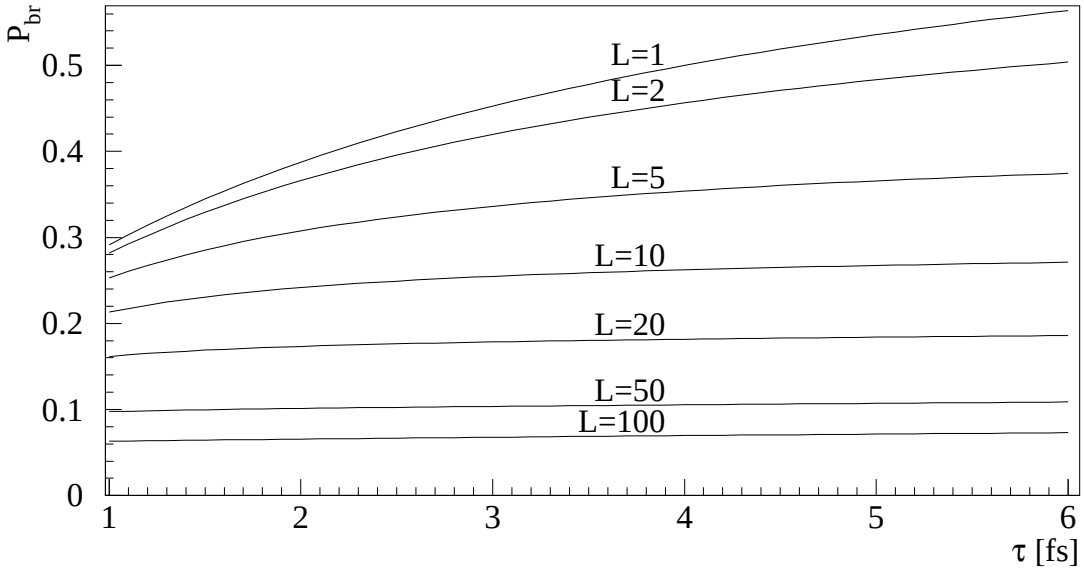

Figure 4: *The probability of $A_{2\pi}$ breakup in the Nickel targets consisting of the different number of layers (L) with 1 mm gap between and having a total thickness of 100 μm as a function of the lifetime τ.*

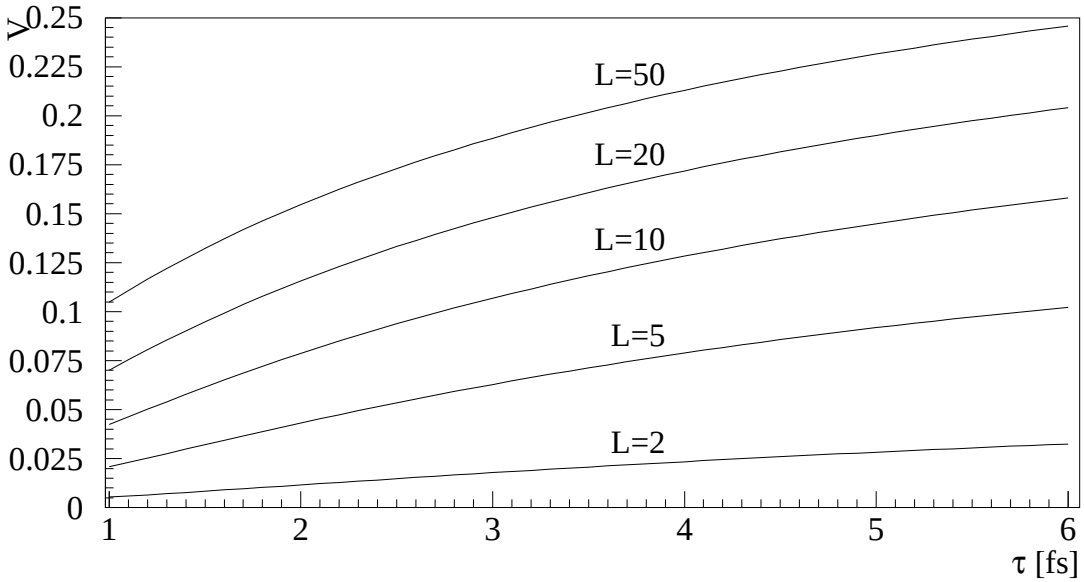

Figure 5: *Variable V defined in Eq.15 as a function of the $A_{2\pi}$ lifetime τ for different number of layers (L).*

method with different numbers of layers in the multi-layer target. The meanings of the rows labels are: "Layers" is the number of layers in the target; "Thickness" is the thickness of one layer in μm; "$P_{\rm br}$" is the theoretical probabilities of the atom breakup in each target at the predicted value of $\tau = (2.9 \pm 0.1) \cdot 10^{-15}$ s (3), V is the function defined in Eq.15; "Relative derivative" is $(dP_{\rm br}/d\tau)/P_{\rm br}$ for the first column and $(dV/d\tau)/V$ for all other; "Statistics" is the multiplication factor for the required raw data to achieve the same statistical accuracy in the lifetime measurement as for the single-target method. For the two-target method it was assumed that total statistics were divided into equal parts for measurements with the single- and multi-layer targets.

Table 2:

Layers	1	5	10	20
Thickness (μm)	100	20	10	5
$P_{\rm br}$	0.447	0.334	0.254	0.178
V		0.061	0.104	0.145
Relative derivative	0.126	0.298	0.241	0.195
Statistics	1.0	2.1	1.1	0.84

From Table 2 we can see that the required amount of raw data with respect to statistical accuracy for the two-target method (with the multi-layer target having the number of layers between 10 and 20) is almost the same or even less as compared to the single-target method. This is result of two reasons. First, $V(\tau)$ function has much high sensitivity to the lifetime τ compared to $P_{\rm br}(\tau)$ which is illustrated by the higher relative derivative. Second, the statistical accuracy of $V(\tau)$ increases with increasing the difference of the numbers in the numerator. Thus with the smaller total number of observed $A_{2\pi}$ we can measure the lifetime with the same accuracy or even better.

Moreover, the results of the fitting procedure described above in Sect. 2.1, which is one of the main source of the systematic errors in the lifetime measurement, enters only to the denominator of $V(\tau)$. It can be shown that in this case its contribution to the lifetime systematic errors is at least by 4 times smaller than in the case of single-target method.

Thus, the two-target method with the number of layers in the multi-layer target between 10 and 20 looks like a very attractive addition to our standard procedure of the lifetime measurement. The target with 12 layers have already been produsedand tested at the DIRAC experiment.

3 Experimental setup

3.1 The DIRAC experimental setup

For the $A_{2\pi}$ lifetime measurement and for observation and lifetime measurement of $A_{\pi K}$ we are going to use the updated DIRAC experimental setup. The existing experimental setup as shown in Fig.6 is located at the 24 GeV/c slow extracted proton beam line of the CERN PS accelerator. The setup is designed to detect charged pion pairs with high resolution over the pair relative momentum.

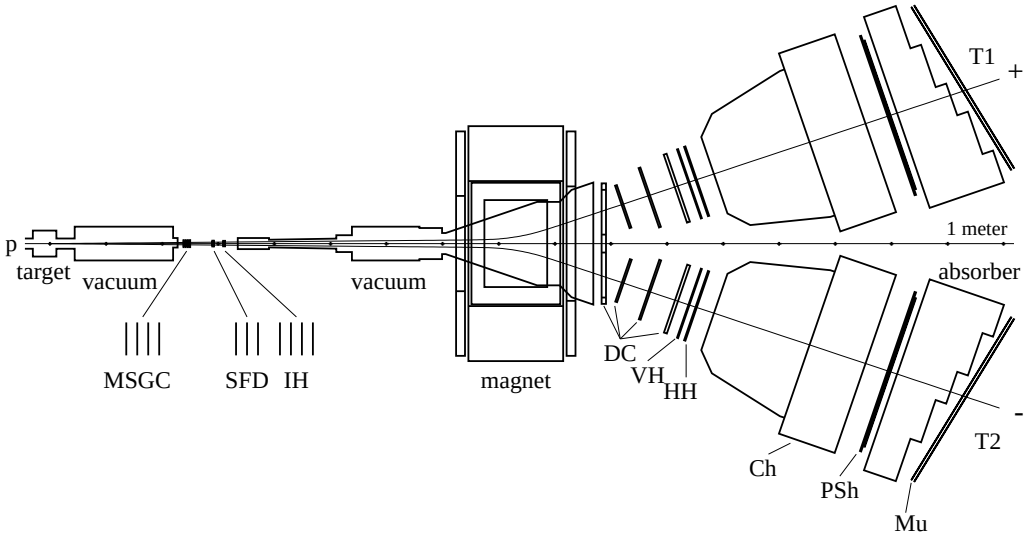

Figure 6: Schematic top view of the DIRAC spectrometer. Upstream of the magnet: microstrip gas chambers (MSGC), scintillating fiber detectors (SFD), ionization hodoscopes (IH). Downstream of the magnet, in each arm of the spectrometer: drift chambers (DC), vertical and horizontal scintillation hodoscopes (VH, HH), gas Cherenkov counter (Ch), preshower detector (PSh) and, behind the iron absorber, muon detector (Mu).

The experiment consists of a target station, a secondary particle vacuum channel, a spectrometer magnet and detectors placed upstream and downstream of the magnet. All the equipment is surrounded by a radiation shielding to protect the outer hall against radiation from the experimental zone.

The proton beam intensity during data taking was $0.9 \cdot 10^{11}$ per spill and the spill duration of 400$\div$450 ms. The target station with 12 holders allows to insert different targets into the beam. Data were collected with Pt, Ni and Ti targets. The target thicknesses are (28, 94 and 247) μm and the corresponding nuclear interaction probabilities ε_{nucl} (3.2, 6.4, 9.0)$\cdot 10^{-4}$, respectively.

"Free" $\pi^+\pi^-$ pairs produced in the target and $\pi^+\pi^-$ pairs from $A_{2\pi}$ breakup in the target ("atomic" pairs) pass into the secondary particle vacuum channel which is tilted upwards by 5.7° with respect to the proton beam. The channel angular aperture of 1.2 msr defined by a collimator. The channel ends with a flat vacuum chamber placed between the spectrometer magnet poles. The outlet window of the chamber is made of 0.68 mm thick Al foil.

The magnet ($B = 1.65$ T, $BL = 2.2$ Tm) and all the detectors are inclined to the proton beam by 5.7° in the vertical plane. The upstream detectors are located in an air gap between the target station and the magnet. They include the microstrip gas chambers (MSGC), the scintillating fiber detectors (SFD) and the scintillation ionization hodoscopes (IH). Downstream of the magnet the setup splits into two arms for positive and negative particle detection and identification. The axes of the arms are at the angles $\pm 19^\circ$ in respect to the secondary beam direction. Each arm includes a set of drift chambers (DC), vertical and horizontal scintillation hodoscopes (VH, HH), a gas Cherenkov counter (Ch), preshower (PSh) and muon detectors (Mu). The momentum range covered by the spectrometer is $1.2 \div 8$ GeV/c.

The upstream detectors with a sensitive area close to 10×10 cm^2 perform tracking before the magnet. The MSGC measure particle coordinates using 4 identical planes: X, Y, U and V, with rotation angles of 0°, 90°, 5°, 85° with respect to the X-plane. The space resolution

for single hits is 54 μm and the efficiency per plane 93%. The SFD provides both coordinate and timing information. It consists of 3 planes for measuring X, Y, and U coordinates. Each plane consists of fiber columns, the fiber diameter being 0.5 mm (KUARAY). Five fibers, forming one sensitive column, are mapped to one channel of the multichannel position sensitive photomultiplier. The 5-fiber column pitch is 0.43 mm. Each plane contains 240 sensitive columns viewed by 15 PSPMs (Hamamatsu H6568). The space resolution is 127 μm (rms) and the time resolution 0.65 ns. The ionization hodoscopes are intended to detect the double ionization signal produced by pion pairs with a very small opening angle, such that the two tracks may be resolved neither in MSGC nor in SFD. The IH detector consists of two staggered vertical (X) and two staggered horizontal (Y) layers, each of 16 slabs with dimensions $110 \times 7 \times 1\,\mathrm{mm}^3$ ($H \times W \times T$).

As first downstream detector the drift chamber system is used to perform particle tracking after the magnet. There are 6 X-, 6 Y- and 2 W-wire planes for coordinate measurements in each arm. The W-wires are inclined at 11.3° with respect to the X-wires. The chambers are assembled in packets: the first one, DC1, common for both arms and the separate packets DC2–DC4 in each arm. A total area of DC1 is $1.6 \times 0.4\,\mathrm{m}^2$ with a central zone of 32 cm made insensitive for the particles. Dimensions of other planes are in the range from $0.8 \times 0.4\,\mathrm{m}^2$ for DC2 to $1.28 \times 0.4\,\mathrm{m}^2$ for DC4. The step of signal wires is 10 mm. The accuracy of coordinate measuments in the DC is better than 90 μm. Each of the vertical hodoscopes is an array of 18 scintillation counters 2.2 cm thick covering a total area of $40 \times 130\,\mathrm{cm}^2$ ($H \times W$). The VH provide the most precise timing among all DIRAC detectors thus defining the time resolution of the setup as a whole. The light is collected to photomultipliers at both ends of the scintillators, and electronic meantimer units are used to exclude the time-on-coordinate dependence. Time resolution of a single vertical hodoscope is 127 ps which corresponds to 174 ps resolution for the time difference between the positive and negative arm signals. The horizontal hodoscopes cover the same area like VH. Each HH consists of 16 horizontal scintillators of $130 \times 2.5 \times 2.5\,\mathrm{cm}^3$ dimensions ($W \times H \times T$). The main purpose of HH is selection at the trigger level of pairs with a small difference of hit slab numbers ("coplanarity cut") typical for the pairs from the pionic atom breakup. The Cherenkov detectors are used for rejection of background of e^+e^- pairs. The gas radiator is nitrogen at normal temperature and pressure. Each counter is equipped with 20 spherical mirrors which focus the Cherenkov light to 10 photomultipliers. The average number of photoelectrons for electrons is over 16 and the efficiency is more than 99.8%. Pion contamination above the detection threshold is estimated to be less than 1.5%. The preshower detectors are installed behind the Cherenkov counters. Each PSh consists of 8 elements, an element comprising a Pb converter and a scintillator. Off-line analysis of the amplitudes from PSh provides an additional e/π separation power. Each muon detector consists of a thick iron absorber followed by two layers of scintillator counters, 28 counters in a layer.

3.2 Trigger and Readout system

The trigger logic provides a reduction of the event rate to a level acceptable to the data acquisition system. Pion pairs are produced in the target mainly in a free state with a wide distribution over their relative momentum Q. The trigger rejects events with pion pairs having $Q_L > 30\,\mathrm{MeV/c}$, $Q_x > 3\,\mathrm{MeV/c}$ and $Q_y > 5\,\mathrm{MeV/c}$ keeping at the same time high efficiency for detection of pairs with Q components below these values. The trigger system [44] comprises a fast first level trigger [45] and higher level trigger processors which apply selection criteria to different components of the relative momentum of pion pairs. In the first level trigger a simple

coincidence logic is used for selection of pion pairs. A coincidence of VH, HH and PSh signals and anticoincidence with Ch signal is treated as a pion event in each arm (muon detector data are analized only off-line). Coincidence of pion signals in both arms, with simultaneously applied at the hardware level the coplanarity cut, initiates the first level trigger. The coplanarity cut puts a limitation to the vertical component Q_y of the relative momentum for the accepted pairs.

Two hardware processors are further used to select pairs with low Q values. One of them is based on a neural network algorithm [46] which employs the hit maps of the IH, SFD and VH detectors. The neural trigger system takes decision in 250 ns, the reduction rate coefficient is around 2. Another processor makes use of the drift chamber data. It reconstructs tracks (by wire numbers) and rejects the events with $Q_L > 30$ MeV/c or $Q_x > 3$ MeV/c. Decision time depends on complexity of the event and is 3.5 μs on average. The reduction rate coefficient is 2.5 with respect to the neural trigger.

The total trigger provides a rate reduction around 5.5 with respect to the first level trigger (or more than 1000 with respect to single rates of the downstream detectors) keeping a high efficiency of 96% in the low Q region of interest. As shown above, for the data analysis purposes the accidental coincidences of particles in the two arms should also be detected. So the trigger is made to accept the accidental particles in the time window $\pm$20 ns as well. All hardware cuts in the trigger processors affect equivalently the real and accidental coincidences. The trigger system provides a parallel accumulation of events of several other processes needed for calibration of the setup: e^+e^- pairs, decays $\Lambda \to p\pi^-$ and $K^\pm \to \pi^\pm\pi^+\pi^-$.

Data readout algorithm is optimized with the beam time structure. In one accelerator supercycle (of 14 to 20 s duration) from 1 to 5 beam spills are delivered to DIRAC. During the spill the data are read out to buffer memories while event building, transfer to the host computer and other software operations take place in the intervals between the spills. This makes possible to accept up to 2000 events per spill of 450 ms at an interval between the spills as short as 1 s (really the event rate in standard conditions was around 700 per spill).

Dedicated readout electronics for MSGC [47] and DC [48] and commercial FERA readout system [49] for all other detectors are used.

3.3 Modification of the setup for the πK atom detection

The method of the $A_{\pi K}$ observation and lifetime measurement is the same as for $A_{2\pi}$: π^+K^- and π^-K^+ "atomic " pairs will be detected simultaneously with $\pi^+\pi^-$ "atomic " pairs. The expected number of detected πK "atomic " pairs for the existing geometry will be by 40 times less than that of $\pi^+\pi^-$. Only $A_{\pi K}$ with momenta higher than 5.8 GeV/c will breakup into detectable πK pairs, namely pairs entering the apparatus acceptance. The pion of the pair will have a momentum range between 1.25 and 2.3 GeV/c, whereas the kaon will have a momentum between 4.6 and 7 GeV/c. The topology of such events for π^+K^- is shown in fig. 7. The high momentum kaon trajectories are close to the setup symmetry axis, whereas the correlated low momentum pions are away from the axis.

In order to detect πK "atomic" pairs one needs to discriminate pions from kaons. We plan to employ Freon 114 having a high refraction index (n=1.0014) at atmospheric pressure as gas radiator in the existing Cherenkov counters instead of N_2 used now. This radiator is suitable to discriminate pions from kaons in the kinematic range of accepted $A_{\pi K}$ since their Cherenkov momentum threshold is 2.6 and 9.3 GeV/c, respectively. Electrons will be separated in the whole setup momentum range. Freon 114 is environmentally safe, non-flammable and can be operated at room temperature, and has a well-understood behaviour from previous experiments.

The detection of $\pi^- K^+$ pairs is somehow more complex as in this case, in addition to π^+, a large admixture of protons to positive kaons is also expected. To achieve an efficient kaon/proton discrimination at trigger level, we will install a small silica aerogel threshold Cherenkov detector in the positive arm. The aerogel detector will be placed between the first (DC1) and second (DC2) drift chamber modules. One module of silica aerogel tiles with average dimensions $150 \times 350 \times 200$ mm^2 (width $\times$ height $\times$ length) would be sufficient to intersect all trajectories of K^+ from $A_{\pi K}$ breakup. The module is viewed by two 5-inches photomultipliers (Hamamatsu R1587) attached to the top and bottom sides. To discriminate between kaons and protons in the kinematical range of $A_{\pi K}$ breakup, aerogel with index of refraction n=1.008 would be the most appropriate. However, extensively tested aerogel tiles only with n=1.01–1.03 are available from the Belle Collaboration at KEK [50]. With n=1.01 the momentum threshold for protons (6.62 GeV/c) is slightly below the maximum momentum of protons entering the apparatus (7.0 GeV/c). Therefore, some Cherenkov light will be emitted by the fastest protons. However, the intensity of the light will be very weak: in 200 mm thick aerogel radiator one expects an average of $3-4$ p.e. from 7.0 GeV/c protons, and about $13-14$ p.e. from kaons with 4.6 GeV/c momentum (minimum momentum from $A_{\pi K}$ breakup). Therefore, we still expect a wide separation region which should allow an efficient proton/kaon separation when operating the detector in the threshold mode. Additional investigations of the properties of silica aerogel with very low index of refraction (n < 1.01) are currently in progress at JINR Dubna, and we intend to exploit both the Japanese and Russian technologies. The dedicated detector is constructed and will be investigated during the test run in 2003.

The existing Cherenkov counters filling with SF_6 gas has already been tested in the experiment and showed a good separation of electrons, pions and kaons. With Freon 114 the separation will be even better.

The implementation of the new detectors will not affect the detection efficiency of $\pi^+\pi^-$ "atomic" pairs. At the existing symmetric geometry we can detect both $\pi^+ K^-$ and $\pi^- K^+$ atoms but with a moderate efficiency because of the big difference in masses of π and K mesons.

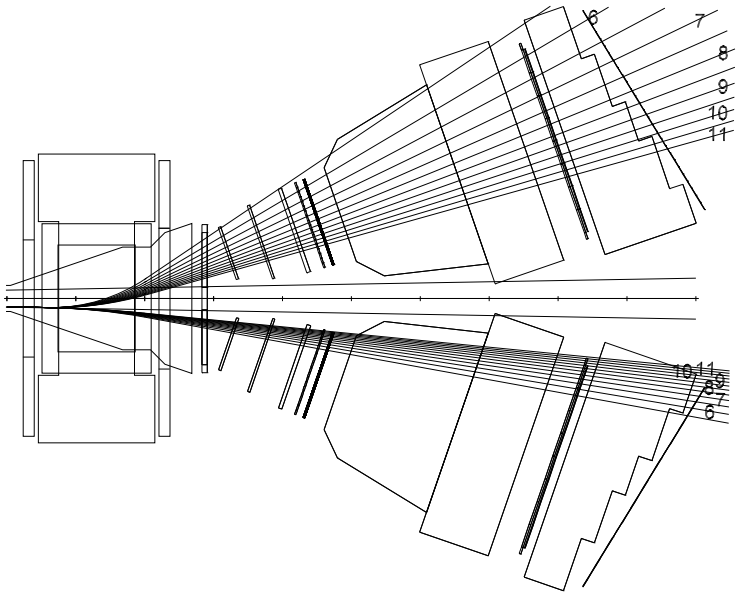

Figure 7: *Trajectories of π^+ and K^- from the $A_{\pi^+ K^-}$ breakup for the existing setup. The labels on the trajectory lines are the $A_{\pi^+ K^-}$ momenta in GeV/c.*

We study now modifications of the downstream detector geometry to improve $A_{\pi K}$ detection efficiency keeping the detection efficiency of $\pi^+\pi^-$ atoms on the acceptable level.

4 Setup modification for experiment at J-PARC

The main difference between CERN PS and J-PARC is very high intensity of the proton beam: $\sim 10^{14}$ protons per spill. So the scheme of DIRAC should be modified to accept such flux. The modifications could include:

- The DIRAC setup should be inclined in vertical plane to the proton beam and installed upstream of all experiments in the K-hall ;
- The single- and multi-layer targets should be introduced into the proton beam halo. We need the number of protons passing through the target about $5 \cdot 10^{11}$ per spill. Because of use of thin targets (nuclear interaction probability less than 10^{-3}) we will not disturb the proton beam for the K-hall;
- The distance between the target and the spectrometer magnet centre will be increased up to 20 m (now this distance is equal to 8.3 m). This will allow us to install a shielding between the intense proton beam and the most part of the setup (now the proton beam passes just under the spectrometer magnet). Also we will need one or two shielding walls upstream of the spectrometer magnet and a shielding wall separating the DIRAC setup from the other experiments in K-hall.
- The part of the setup from the target station up to the spectrometer magnet (about 20 m) will have small transverse dimensions. So this part may be placed in a tunnel upstream of the K-hall;
- The spectrometer magnet and the downstream detectors (full longitudinal dimension is about 10 m) should be placed in the beginning of the K-hall.

Probably some other modifications will be required also.

For the future DIRAC experiment at J-PARC the following improvements could be foreseen:

- The measurements with single- and multi-layer targets to decrease significantly the systematic errors;
- Installation of two permanent magnets near the target. The small permanent magnet with $BL = 0.012$ Tm (0.25 T for a length of s 50 mm) behind the target will decrease the systematic errors arising for the "closed track" reconstruction. Because both the proton and secondary beams will pass through this magnet we need to install a second permanent magnet upstream of the target with inverse polarity to keep the correct proton beam direction for the K-hall users. One of the permanent magnets has been manufactured already in Japan [51].
- Supplementary new SFD planes (two planes of $50 \times 50\,\mathrm{mm}^2$) will improve the particle detection efficiency by 20% or more. This detector is being manufactured now.

- Micro Drift Chambers (18 planes, $80 \times 80\,\mathrm{mm}^2$) will be installed upsteam of existing SFD. They will improve the track reconstruction in the upstream part and the off-line suppression of the background not generated in the target. This detector is being manufactured now.

- A Si detector for dE/dx measurement ($90 \times 90\,\mathrm{mm}^2$) can be installed to improve the two particle separation. The prototype of this detector exists [52].

All these modifications will increase the setup efficiency and considerably suppress the influence of known sources of systematic errors.

5 Other physics subjects

5.1 Observation of $A_{2\pi}$ long-lived states

Strong interaction and vacuum polarisation lead to a splitting of $A_{2\pi}$ energy levels and hence to a difference ΔE_{ns-np} between ns and np energy levels — Lamb shif. For $n = 2$ the value ΔE_{2s-2p}, resulting from the strong interaction, is proportional to $(2a_0 + a_2)$. Thus, the simultaneous measurements of the $A_{2\pi}$ lifetime and the Lamb shift allows to obtain a_0 as well as a_2 in a model-independent way.

In order to measure ΔE_{ns-np}, the dependence of the lifetime of long-lived $A_{2\pi}$ states ($l \neq 0$) on the applied electric field should be studied [31, 53, 54]. Calculations show that up to $\sim 10\%$ of the atoms, generated in the thin target, reach the vacuum region as long-lived states [16]. Such $A_{2\pi}$ atoms may be observed in the DIRAC setup without any change, and the results could demonstrate the feasibility of ΔE_{ns-np} measurement.

5.2 Study of charged particle production dynamics using Coulomb correlation

The study of the $\pi^+\pi^-$ Coulomb correlation enables to measure the fractions of pion pairs generated by short-lived (ρ, ω, $\Delta\ldots$) or by long-lived sources (η, $\eta\prime\ldots$) [55]. This relation can be measured as a function of the pair energy in the lab system at the few percent level. The identification of K^-, K^+ and p allows to perform the same analysis for further combinations of charged particles. The Coulomb correlations for K^+K^- and K^-p are sensitive to the size of their production region. Therefore the correlation study allows to obtain a picture of this particle production dynamics in coordinate space for light and heavy nuclei.

5.3 Bose-Einstein correlations

A study of the Bose-Einstein correlations in $\pi^-\pi^-$ and $\pi^+\pi^+$ requires the consideration of Coulomb corrections for those pairs, which originate from short-lived sources [56]. Exploiting the high relative momentum resolution of our spectrometer, it should be possible to extract these corrections from the measurements ($\pi^-\pi^-$, $\pi^+\pi^+$ and $\pi^+\pi^-$) themselves. The data for like-sign particles are taken as a by-product during normal data acquisition.

6 Information about collaboration

The authors of this Letter of Intent are the members of the DIRAC collaboration at CERN (PS212). The goal of DIRAC at CERN was to measure the $A_{2\pi}$ lifetime. Nowaday about 12000 $\pi^+\pi^-$ pairs originated from the $A_{2\pi}$ breakup were identified and the expected accuracy of the lifetime is about 14%. The CERN authorities plan to stop the experiment in 2003 in order to focus on the LHC construction. So we are looking for a possibility to continue our experiment with $\pi^+\pi^-$ atoms to reach the accuracy of modern theoretical predictions and furthermore to observe and study the πK atom. A major part of the existing detectors and dedicated electronics can be used in the proposed experiment.

References

[1] S. Deser et al., Phys. Rev. 96 (1954) 774.

[2] J. Uretsky and J. Palfrey, Phys. Rev. 121 (1961) 1798.

[3] S.M. Bilenky et al., Yad. Phys. 10 (1969) 812; (Sov. J. Nucl. Phys. 10 (1969) 469).

[4] H. Jallouli and H. Sazdjian, Phys. Rev. D58 (1998) 014011; Erratum: ibid., D58 (1998) 099901.

[5] M.A. Ivanov et al. Phys. Rev. D58 (1998) 094024.

[6] J. Gasser et al., Phys.Rev. D64 (2001) 016008; hep-ph/0103157.

[7] A. Gashi et al., Nucl. Phys. A699 (2002) 732.

[8] S. Weinberg, Physica A96 (1979) 327; J. Gasser and H. Leutwyler, Phys.Lett. B125 (1983) 325; ibid Nucl. Phys. B250 465, 517, 539.

[9] G. Colangelo, J. Gasser and H. Leutwyler, Phys. Lett. B 488 (2000) 261.

[10] G. Colangelo, J. Gasser and H. Leutwyler, Nucl. Phys. B603 (2001) 125.

[11] G. Colangelo, J. Gasser and H. Leutwyler, Phys. Rev. Lett. 86 (2001) 5008.

[12] M. Knecht et al., Nucl. Phys. B457 (1995) 513.

[13] L. Rosselet et al., Phys. Rev. D15 (1977) 547.

[14] See compilation of Nagels M.M. et al., Nucl. Phys. 147 (1979) 189, and references mentioned therein.

[15] S. Pislak et al., Phys. Rev. Lett, 87 (2001) 221801.

[16] B. Adeva, *et al.*, CERN/SPSLC 95–1, SPSLC/P 284, Geneva 1995; http://cern.ch/dirac.

[17] S. M. Bilenky *et al.*, Yad. Fiz. 10 (1969) 812;

[18] V. E. Lyubovitskij, E. Z. Lipartia and A. G. Rusetsky, Pis'ma Zh. Exp. Teor. Fiz **66** (1997) 747.

[19] H. Jallouli and H. Sazdjian, Phys. Rev. D58 (1998) 014011; 099901(E).

[20] M. A. Ivanov, V. E. Lyubovitskij, E. Z. Lipartia and A. G. Rusetsky, Phys. Rev. D58 (1998) 0094024.

[21] A. Gall, J. Gasser, V. E. Lyubovitskij and A. Rusetsky, Phys. Lett. **B462** (1999) 335.

[22] J. Gasser, V. E. Lyubovitskij and A. G. Rusetsky, Phys. Lett. **B471** (1999) 244.

[23] J. Gasser and A. G. Rusetsky private comunication.

[24] U. Moor, G. Rasche and W. S. Woolcock, Nucl. Phys. A587 (1995) 747.

[25] A. Gashi *et al.*, Nucl. Phys. A628 (1998) 101.

[26] V. Bernard, N. Kaiser and U. Meissner, Phys. Rev. D43 (1991) 2757;
V. Bernard, N. Kaiser and U. Meissner, Nucl. Phys. B357 (1991) 129.

[27] A. Roessl, Nucl. Phys. B555 (1999) 507; (hep-ph/9904230).

[28] C. B. Lang, Nuovo Cimento **41A** (1977) 73.

[29] N. Johannesson and G. Nilsson, Nuovo Cimento 43A (1978) 376.

[30] A. Karabarbouris and G. Shaw, Journal of Phys. G6 (1980) 583.

[31] L. L. Nemenov, Yad. Fiz 41 (1985) 980; Sov. J. Nucl. Phys. 41 (1985) 629.

[32] A. D. Sakharov, Zh. Eksp. Teor. Fiz. 18 (1948) 631.

[33] V. N. Bayer and V. S. Fadin, Zh. Eksp. Teor. Fiz. 57 (1969) 225;
Sov. Phys. JETP 30 (1970) 120.

[34] L. G. Afanasyev, O. Voskresenskaya and V. Yazkov, JINR preprint, P1-97-306, Dubna, 1997.

[35] L. G. Afanasyev and O. Voskresenskaya, Phys. Lett. B453 (1999) 302.

[36] L. G. Afanasyev et al., Phys. Lett. 308B (1993) 200.

[37] L.G. Afanasyev and A.V. Tarasov, Yad.Fiz. 59 (1996) 2212; (Phys. At. Nucl. 59 (1996) 2130).

[38] Z. Halabuka et al., Nucl.Phys. B554 (1999) 86–102.

[39] L. Afanasyev, A. Tarasov and O. Voskresenskaya, J.Phys. G 25 (1999) B7.

[40] T.A. Heim et al., J. Phys. B: 33 (2000) 3583.

[41] T.A. Heim et al., J. Phys. B: 34 (2001) 3763.

[42] M. Schumann et al., J. Phys. B: 35 (2002) 2683.

[43] L. Afanasyev, A. Tarasov and O. Voskresenskaya, Phys.Rev.D 65 (2002) 096001; hep-ph/0109208.

[44] L.Afanasyev et al., NIM A491 (2002) 376–389.

[45] L.Afanasyev, M.Gallas, V.Karpukhin, A.Kulikov., NIM A479 (2002) 407–411.

[46] P.Kokkas, M.Steinacher, L.Tauscher, S.Vlachos., NIM A471 (2001) 358–367.

[47] F.Gomez, P.Vasques. *MSGC/GEM detector electronics.* DIRAC Note 2000-01, CERN, 2000.

[48] L.Afanasyev, V.Karpukhin. NIM A 492 (2002) 351–355; arXiv:hep-ex/0208011.

[49] *Fast Encoding and Readout ADC System Possibilities.* Application Note AN-4004A, LeCroy Corporation.

[50] T. Sumiyoshi *et al.*, Nucl. Instr. and Meth. A433 (1999) 385.

[51] M. Chiba, A. Kuptsov, K. Okada *Small analyzing magnet*, DIRAC Note 2001-06, CERN, 2001.

[52] M. Kobayashi *et al.*, Nucl. Instr. and Meth. A487 (2002) 353-364.

[53] L. L. Nemenov and V. D. Ovsyannikov, Phys. Lett. B 514 (2001) 247.

[54] L. L. Nemenov, V. D. Ovsyannikov and E. V. Chaplygin, Nucl. Phys. A 710 (2002) 303.

[55] L. G. Afanasyev et al., Phys.Lett.B, 255 (1991) 146.

[56] R. Lednicky and V. L. Lyuboshits, Yad. Fiz. 35 (1982) 1316; Sov. J. Nucl. Phys. 35 (1982) 770.